THE JOURNAL OF PHYSICAL CHEMISTRY C

Article

Cite This: J. Phys. Chem. C 2019, 123, 21415−21421

pubs.acs.org/JPCC

Effect of Surface Ligand on Charge Separation and Recombination at $CsPbI_3$ Perovskite Quantum Dot/TiO_2 Interfaces

Published as part of The Journal of Physical Chemistry virtual special issue "Hai-Lung Dai Festschrift".

Qiongyi Shang,[†] Brandon D. Piercy,[‡] Mark D. Losego,[‡] and Tianquan Lian*[,†]

[†]Department of Chemistry, Emory University, Atlanta, Georgia 30322, United States

[‡]School of Materials Science and Engineering, Georgia Institute of Technology, Atlanta, Georgia 30332, United States

Supporting Information

ABSTRACT: $CsPbI_3$ perovskite quantum dot (QD) solar cells are a promising device platform for further development due to their improved stability compared to bulk materials. The fabrication of these devices often involves postsynthetic washing of colloidal QDs to remove surface ligands. Herein, we investigate how this postsynthetic treatment affects the charge separation (CS) and charge recombination (CR) processes at the interface of $CsPbI_3$ QDs and the TiO_2 electron extraction layer. The CS time constant at QD/TiO_2 interface decrease from 457 ± 4 ps for QDs directly deposited on TiO_2 to 288 ± 1 ps for QDs that were washed twice by methyl acetate, increasing the ET efficiency from 89.9 ± 0.3% to 98.3 ± 0.01%. Interestingly, this treatment also lengthens the average charge recombination time constants from 346 ± 18 ns to 1180 ± 60 ns, which is also beneficial for reducing charge recombination loss. This result demonstrates the pronounced effect of QD washing by methyl acetate (MeOAc) on interfacial charge transfer processes, suggesting the important effect of postsynthesis modification of colloidal perovskite QDs on solar cell efficiencies.

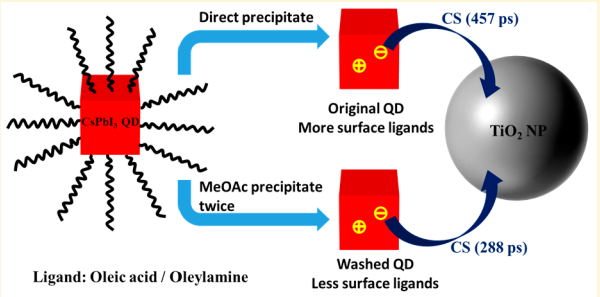

INTRODUCTION

Methylammonium lead halide ($MAPbX_3$) perovskite photovoltaic devices have achieved tremendous success with reported power conversion efficiencies exceeding 20%.[1,2] However, the low stability of organic−inorganic hybrid perovskite materials limits their commercial implementation.[1,3−5] Incorporating inorganic cations (Cs^+ or Rb^+) in bulk perovskite films[6−8] and using all-inorganic perovskite quantum dots[9−11] are possible options to improve device stability. The cubic phase of $CsPbI_3$ can be stabilized at room temperature in quantum dot (QD) form for months, and the efficiency of $CsPbI_3$ QD solar cells (13.43%)[12] can exceed that of nonperovskite QD solar cells, suggesting great promise for perovskite QD-based solar cell technology.[1,13]

The overall solar to electricity conversion process of perovskite QD solar cells involves many elementary processes, such as carrier transport within the QD film, carrier transfer at the interface with electron and hole extraction layers, and competing charge recombination processes. The optimization of the rates of these processes is key to the rational improvement of device performance. In recent reports of $CsPbI_3$ QD photovoltaic devices, a postsynthesis purification method using methyl acetate (MeOAc) as antisolvent to precipitate QDs was found to improve the device performance,[9,12] compared to devices prepared with QDs purified with a direct precipitation method.[14] It was reported that after washing by MeOAc two times most surface ligands on QDs are removed.[9] These findings may suggest the important role of QD surface ligand density in the overall device performance. The organic surface ligands may lower the charge transport between QDs and slow down interfacial charge transfer between QDs and electron- and hole-accepting layers. Although efficient charge transfer between perovskite QDs to TiO_2 films has been studied previously,[15,16] the influences of ligand quantity and purification methods on the charge separation and recombination rates have not been reported.

Herein, we study the effect of postsynthesis treatment of QDs on the dynamics of charge separation (CS), i.e., photoinduced electron transfer (ET) from excited QDs to TiO_2, and charge recombination, i.e., back ET from TiO_2 to QDs, between $CsPbI_3$ perovskite QDs and TiO_2 (NP) films (see eq 1 and Scheme 1).

$$\begin{aligned} &CsPbI_3(e-h) + TiO_2 \\ &\xrightarrow{CS} CsPbI_3(h) + TiO_2(e) \\ &\xrightarrow{CR} CsPbI_3 + TiO_2 \end{aligned} \quad (1)$$

Fourier-tranform infrared (FTIR) spectroscopy measurements reveal that the amount of ligands in the QD/TiO_2 films

Received: July 15, 2019
Revised: August 12, 2019
Published: August 13, 2019

DOI: 10.1021/acs.jpcc.9b06725
J. Phys. Chem. C 2019, 123, 21415−21421

Scheme 1. Schematic Energy Level Diagram and Charge Separation and Recombination Pathways at the $CsPbI_3$ QD/TiO_2 NP Interface: Conduction Band (CB) and Valence Band (VB) Edges in $CsPbI_3$, TiO_2, and Al_2O_3 (Black Horizontal Solid Lines), Charge Separation (CS) from QD to TiO_2 (Dark Blue Arrows), Charge Recombination (CR) Process (Green Arrow), and Electron−Hole Recombination Inside the QD (Dashed white Arrow)

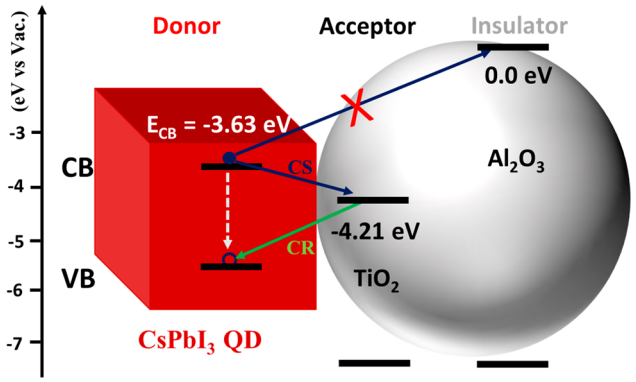

decreases with the extent of postsynthesis washing of QDs by MeOAc. By transient absorption (TA) spectroscopy, we observed that both charge separation and recombination rates between the QDs and TiO_2 are affected by the postsynthesis treatment, suggesting potential impact on solar cell efficiencies.

METHODS

Sample Preparations. $CsPbI_3$ QDs were synthesized according to a published hot injection method.[9,14,17,18] First, Cs-oleate precursor stock solution was prepared by loading 0.203 g of Cs_2CO_3, 0.63 mL of oleic acid (OA), and 10 mL of octadecene (ODE) into a 25 mL three-neck flask and heating them to 150 °C under Ar atmosphere until getting clear solution. The precursor solution was kept at 100 °C to avoid the precipitation of Cs-oleate. In another 100 mL three-neck flask, 0.5 g of PbI_2 and 25 mL of ODE were heated at 120 °C under Ar flow for 30 min. 2.5 mL of OA and 2.5 mL of oleylamine (OAm) were injected at 120 °C to dissolve the PbI_2. The solution was heated to 175 °C, and 2 mL of Cs-oleate precursor solution was injected swiftly. After 5 s, the reaction was quenched by an ice−water bath. The as-synthesized QDs contain a mixture of oleic acid (OA) and oleylamine (OAm) ligands on their surfaces,[14] and a recent study shows that the dominant surface ligands are alkylammonium halide.[19] Two batches of QDs with different ligand coverage were obtained through different postsynthesis treatments, denoted as QD original and QD washed in the figures, respectively. To obtain the original QD sample, the crude solution was centrifuged at 5500 rpm for 15 min to precipitate the aggregated QDs. After centrifugation, the precipitate was dispersed in heptane for further use. To obtain the washed QD sample, methyl acetate (1:1 volume) was added into the crude solution, followed by centrifugation at 5500 rpm for 15 min. The precipitate was dissolved by 1 mL of hexane in each centrifuge tube (6 in total). Another 1 mL of methyl acetate was added into each tube, followed by centrifugation at 5500 rpm for 10 min. The precipitate was dispersed in heptane for future use. Both the original and washed samples were centrifuged to remove aggregates in solution before use.

TiO_2 nanocrystalline thin films were fabricated by doctor-blading colloidal dispersions (NP diameter 30 nm) onto sapphire substrates and annealing at 450 °C for 1 h.[27−30] TiO_2 films coated with ∼1.3 nm Al_2O_3 films via atomic layer deposition (ALD) were used as control systems, in which the higher CB band edge of Al_2O_3 prevents electron injection from QDs.[31,32] These films are referred to as Al_2O_3@TiO_2 hereafter. To prepare QDs on sapphire windows, concentrated QD solutions were spin coated on sapphire windows at 2000 rpm for 20 s. To prepare QD-sensitized TiO_2 and Al_2O_3@TiO_2 samples, bare films were immersed in concentrated $CsPbI_3$ QD solution for 48 h,[27] followed by a heptane rinse to remove weakly adsorbed QDs on the films.

Visible Femtosecond Transient Absorption. The pump−probe transient absorption (TA) experiments were based on a regeneratively amplified Ti:sapphire laser system (Coherent Legend, 800 nm, 150 fs, 2.3 mJ/pulse, and 1 kHz repetition rate). The femtosecond TA measurements were performed with a Helios spectrometer (Ultrafast Systems LLC). 500 nm pump pulses were generated by sum-frequency generation at the BBO crystal using the 1333 nm signal of an optical parametric amplifier (OPA, Opera, Coherent) and the 800 nm laser beam. The power of the pump beam was adjusted by a neutral-density filter. The pump beam was collimated and then focused at the sample with a beam waist of 300 μm. A white-light continuum (WLC) from 420 to 800 nm was generated by focusing ∼10 μJ of the 800 nm pulse into a sapphire window. The WLC was split into probe and reference beams. The probe beam was collimated and then focused with an Al parabolic reflector onto the sample (with a beam waist of 150 μm at the sample). Both the reference and probe beams were sent into a fiber-optics-coupled multichannel spectrometer with complementary metal-oxide-semiconductor (CMOS) sensors and detected at a frequency of 1 kHz. The reference beam intensity was used to correct the pulse-to-pulse fluctuation of the white-light continuum. The pump beam was chopped by a chopper synchronized to 500 Hz. The pump-induced absorbance change was calculated by comparing the probe intensities of the pumped and unpumped samples. The delay time between the pump and probe pulses was controlled by a motorized delay stage. The instrument response function (IRF) of this system was determined to be ∼150 fs by measuring solvent responses under the same experimental conditions (with the exception of a higher excitation power).

Visible Nanosecond Transient Absorption. Nanosecond TA experiments were conducted with the EOS spectrometer (Ultrafast Systems LLC). The pump beams were generated in the same way as the femtosecond TA measurements. The white-light continuum (380−1700 nm, 0.5 ns pulse width, 20 kHz repetition rate) used here was generated by focusing a Nd:YAG laser into a photonic crystal fiber. The delay time between the pump and probe beam was controlled by a digital delay generator (CNT-90, Pendulum Instruments). The probe and reference beams were detected with the same multichannel spectrometers used in the femtosecond TA experiments. To connect spectra and kinetics from femtosecond and nanosecond TA measurements, we scaled the amplitudes of the nanosecond data by a factor to overlap with the femtosecond data in the delay time from 0.7 to 1 ns.

DOI: 10.1021/acs.jpcc.9b06725
J. Phys. Chem. C 2019, 123, 21415−21421

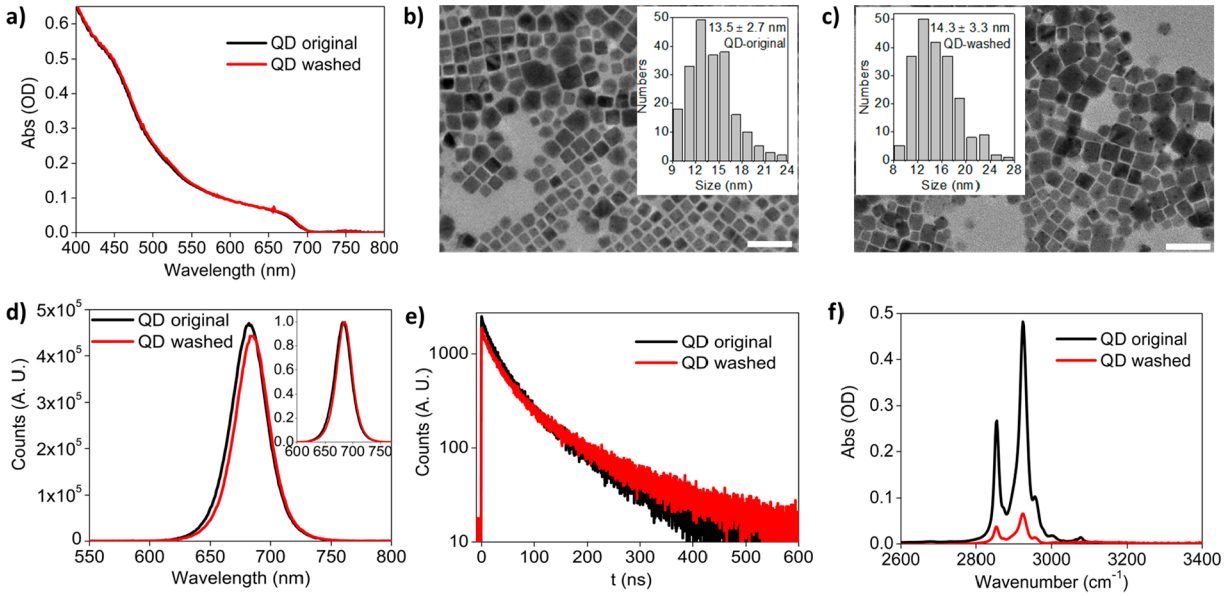

Figure 1. Spectroscopic and TEM characterization of QDs. (a) UV−vis absorption spectra of original QDs and washed QDs in hexane. (b) and (c) TEM images of original and washed QDs. Scale bar: 50 nm. Insets are size distribution statistics. (d) PL spectra of QD solutions in (a). Inset: normalized spectra. (e) PL decay kinetics of QD solutions in (a), excited at 490 nm. (f) FTIR spectra of original and washed QDs spin-coated on sapphire windows. The absorbance has been normalized to the QD absorbance at 680 nm to correspond to the same amount of QDs on these films.

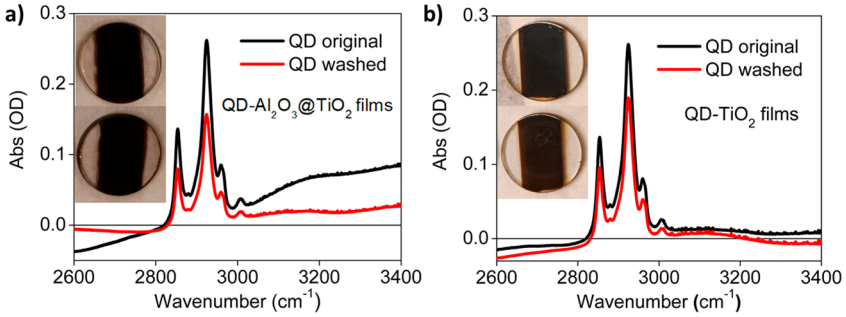

Figure 2. FTIR spectra of QDs on (a) Al_2O_3@TiO_2 and (b) TiO_2 films prepared with (QD washed) and without (QD original) postsynthesis MeOAc wash of QDs. The amplitudes have been scaled by QD absorance at 680 nm to compare the relative ligand quantities. Insets are photos of the QD sensitized films.

Time-Resolved PL Decay Measurements. The time-correlated single-photon counting (TCSPC) technique was adopted to measure the fluorescence decay kinetics. The excitation pulses at 490 nm were generated by frequency doubling of the output pulses centered at 980 nm (~100 fs, 80 MHz) from a mode-locked Ti:Sapphire laser (Tsunami oscillator pumped by a 10 W Millennia Pro, Spectra-Physics) through a BBO crystal. The emitted photons from QDs were detected by a microchannel-plate photomultiplier tube (Hamamatsu R3809U-51), whose output was amplified and analyzed by a TCSPC board (Becker & Hickel SPC 600). The IRF of this system was determined to be ~200 ps.

RESULTS AND DISCUSSION

The absorption and emission spectra of both $CsPbI_3$ QDs in heptane (Figure 1a and 1d) show band gaps at ~1.81 eV and broad absorption across most of the visible spectrum. The photoluminescence quantum yields (PL QYs) are 24.2% and 21.7% for QD original and QD washed, respectively, and PL decay kinetics (Figure 1e) vary only slightly for these two batches of QDs. This finding may be consistent with the reported defect tolerance of $CsPbI_3$ QDs.[19] Consistent with previous reports,[9,14,17,18,20,21] these QDs have a cubic crystal phase and exhibit cuboidal shapes in TEM images (Figure 1b and 1c) with average edge lengths of 13.5 ± 2.7 nm and 14.3 ± 3.3 nm, for the original and washed QDs, respectively. The reported valence band (VB) positions of $CsPbI_3$ bulk crystals (~−5.4 V vs vacuum)[22,23] and QDs[24] (−5.44 V vs vacuum) are similar because of the weak quantum confinement in these QDs. The conduction band (CB) edge position is estimated to be −3.63 V from the known band gap (1.81 eV) by neglecting the weak e−h Coulomb binding energy (~20 meV[14]). The CB positions of TiO_2 NPs were reported to be −4.21 V versus vacuum at the point of zero charge (pH 5.8)[25,26] (Scheme 1). Therefore, the corresponding driving forces for ET and CR are ~0.58 and ~1.23 eV at the QD/TiO_2 interface, respectively. Figure 1f shows a comparison of normalized infrared (IR) absorption spectra of QDs spin-coated on sapphire windows prepared with the original and washed QDs. The normalization factors are determined by their absorbance at 680 nm, such that the normalized IR spectra correspond to the same amount of QDs on the films. The film prepared from the

DOI: 10.1021/acs.jpcc.9b06725
J. Phys. Chem. C 2019, 123, 21415−21421

Table 1. IR/Vis Values of Different Films[a]

films	QD original-sapphire	QD original-Al_2O_3@TiO_2	QD original-TiO_2	QD washed-sapphire	QD washed-Al_2O_3@TiO_2	QD washed-TiO_2
IR/Vis	4.120	0.594	0.848	0.565	0.356	0.616

[a]IR/Vis is the ratio of the IR absorbance of the ligand at 2925 cm^{-1} to the visible absorbance of QDs at 680 nm (Table S1), which represents the relative amount of ligands per QD.

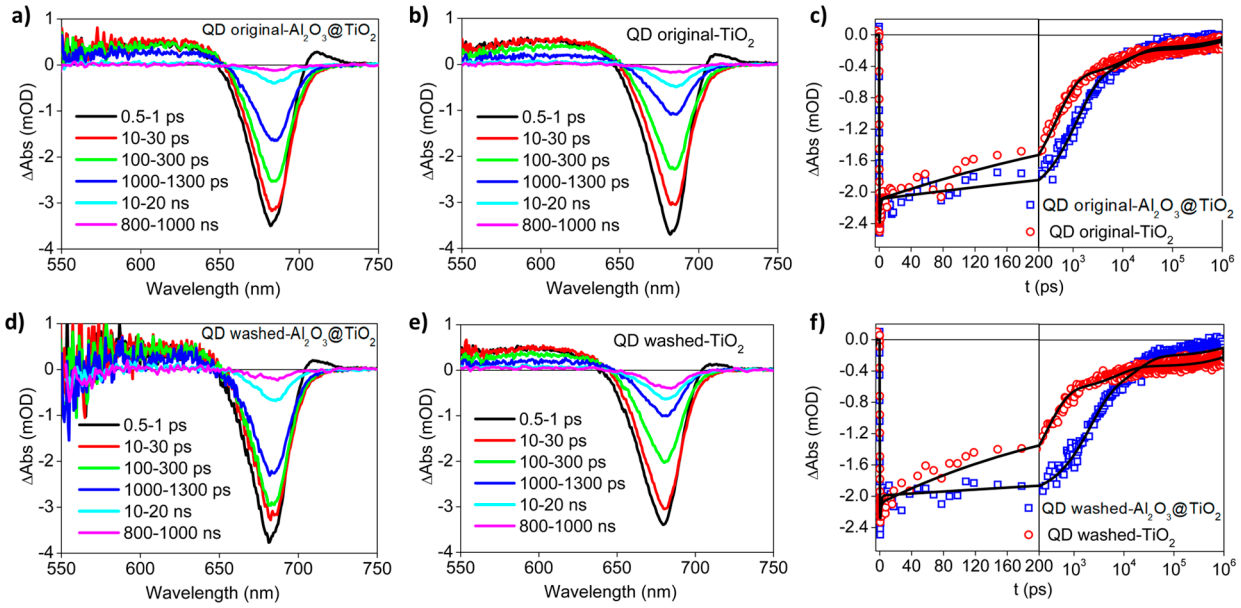

Figure 3. TA spectra and kinetics of $CsPbI_3$ perovskite QDs on metal oxide films measured with 500 nm excitation. TA spectra of original QDs on (a) Al_2O_3@TiO_2 and (b) TiO_2 films at indicated time delays after 500 nm excitation. (c) Comparison of XB recovery kinetics of original QDs on Al_2O_3@TiO_2 (blue squares) and TiO_2 (red circles) films. TA spectra of washed QDs on (d) Al_2O_3@TiO_2 and (e) TiO_2 films at indicated time delays after 500 nm excitation. (f) Comparison of XB recovery kinetics of washed QDs on Al_2O_3@TiO_2 (blue squares) and TiO_2 (red circles) NP films. Black solid lines are multiexponential fits according to the model provided in the SI.

washed QDs shows lower IR absorbance in the CH stretching mode region,[9] indicating lower ligand coverage in these films.

Adsorption of QDs on TiO_2 and Al_2O_3@TiO_2 films was confirmed by color change (Figure 2 insets) and UV/vis absorption spectra (Figure S1) of QD-TiO_2 and QD- Al_2O_3@TiO_2 films. Fourier transform IR spectra were measured to determine the ligand absorption on the films (Figure 2). It was difficult to control the amount of QDs on these films (Table S1) due to differences in the films and QD solutions (ligand coverage and concentration). To account for this variation, we use the ratio of the IR absorbance of the peak at 2925 cm^{-1} and the visible absorbance at 680 nm (IR/Vis) as the measure of total ligand quantity relative to the QD quantity on QD/TiO_2 films because the IR and visible absorbances are proportional to the amount of ligands and the number of QDs, respectively. These values are listed in Table 1. Note that these ligands can also adsorb on TiO_2 and Al_2O_3@TiO_2 films (Figure S2) and may contribute to the total ligand amount shown in Figure 2. As shown in Table 1, compared with QDs on the sapphire, QDs originally suffered significant ligand loss when adsorbed into TiO_2 and Al_2O_3@TiO_2 films. This difference in ligand amount is likely caused by different sample preparation methods. The latter samples were washed by heptane during the preparation process, which may remove some of the ligands. Furthermore, the latter sample was prepared by soaking TiO_2 and Al_2O_3@TiO_2 films in QD solution films for 48 h, a process that may selectively adsorb QDs with lower ligand coverage. Such selective adsorption is unlikely in QD/sapphire samples (Figure 1f) prepared by spin coating. However, both the QD original-Al_2O_3@TiO_2 and QD original-TiO_2 had higher IR/Vis values than the QD washed-Al_2O_3@TiO_2 and QD washed-TiO_2, respectively, as shown in Figure 2 and Table 1.

Ultrafast TA spectroscopy measurements were conducted to investigate the CS and CR processes. The details of pump–probe TA setups have been described in the Methods section. Figure 3a, b, d, and e shows the TA spectra of $CsPbI_3$ QDs on Al_2O_3@TiO_2 and TiO_2 films. The TA spectra are dominated by an exciton bleach (XB) feature peaked at ~680 nm, caused by the state filling of the CB electron and VB hole at the band edges.[33] The recovery of XB signal can be used to follow the electron and hole dynamics.

To quantify the electron and hole contributions to the XB signal, we also studied TA spectra and kinetics of QD-Rhodamine B (RhB) complexes in which RhB serves as a selective electron acceptor (Figures S3 and S4). Details are provided in the SI (S3). The result shows that in $CsPbI_3$ QDs, the state fillings of electron and hole contribute ~51.6% and 48.4%, respectively, to the XB feature (Table S2). These contributions are different from $CsPbBr_3$ QDs (67.2% and 32.8%).[33] The result is consistent with the reported similar effective masses of the electron and hole in bulk $CsPbI_3$ ($0.11m_0$ and $0.13m_0$, respectively; m_0 is the mass of free electron).[14] For the original QDs and washed QDs in solution, the electron contributions are measured to be 53.1% and 57.2%, respectively (Figures S5 and S6 and Table S3 and S4).

The XB recovery kinetics of QDs on Al_2O_3@TiO_2 and TiO_2 films are compared in Figure 3c and 3f for original and washed

DOI: 10.1021/acs.jpcc.9b06725
J. Phys. Chem. C 2019, 123, 21415–21421

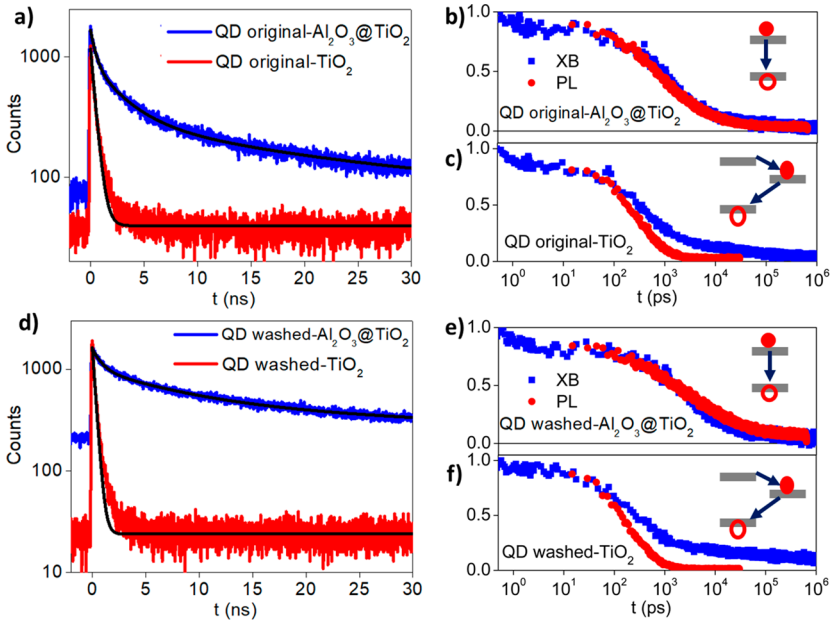

Figure 4. Comparisoin of PL decay and XB recovery kinetics of $CsPbI_3$ QDs on NP films. Comparison of PL decay on Al_2O_3@TiO_2 and TiO_2 for (a) QD original and (d) QD washed samples. Black solid lines are fits of PL decays described in the SI (S4). Comparison of PL decay (red) and XB kinetics (blue) of QDs on NP films for QD originals (b, c) and QD washed (e, f) on TiO_2 (c,f) and Al_2O_3@TiO_2 (b,e). Insets in b,c,e,f: dominant processes in these films: exciton recombination within QDs (in b,e) or interfacial CS followed by CR (in c, f).

QDs, respectively. Compared to QDs on Al_2O_3@TiO_2, the XB decay of QDs on TiO_2 shows a faster decay on the <10 ns time scale and a slower decay on the >10 ns time scale. This is consistent with a fast electron transfer to TiO_2 and slow hole decay (by charge recombination with the transferred electron in TiO_2) expected from band alignment shown in Scheme 1. To further confirm the above assignment, time-resolved photoluminescence (PL) decay kinetics were measured for the same samples. As shown in Figure 4a and d, the PL decays are accelerated for QDs on TiO_2 compared to Al_2O_3@TiO_2, consistent with the presence of the ET quenching pathway in the former samples. Because PL decay probes the exciton (e−h pair) dynamics, complete decay of the CB electron (or VB hole) by any pathways (e−h recombination, electron trapping, or ET to TiO_2) leads to a complete PL decay. On the other hand, XB bleach probes the sum of electron and hole population, and complete decay of CB electron by ET to TiO_2 only leads to a partial decay of XB signal (with the hole contribution remaining). Thus, it is informative to compare the PL decay and XB bleach kinetics (Figure 4b, c and e, f), although the PL decay curves miss data points at short delay time (<10 ps) due to a lower time resolution of PL measurement. For QDs on Al_2O_3@TiO_2 (Figure 4b and e), the PL decay and XB kinetics match well with each other, indicating that electron−hole recombination dominates the excited state decay, consistent with the expected lack of interfacial electron transfer in this sample.

For QDs on TiO_2 films (Figure 4c and f), a normalized comparison of XB bleach and PL decay shows that PL decay and XB decay agree with each other at <1 ns (Figure S7), and there exist slow XB recovery components at >1 ns (Figure 4c and f). These results are consistent with ET from QD to oxides, which leads to complete (and fast) PL decay and the formation of a charge-separated state. In the charge-separated state, the VB hole remaining in the QD is responsible for the longer lived XB signal, the decay of which can be used to follow the charge recombination process (Scheme 1).

Based on the above analysis, we used a multiexponential fitting model to extract the charge separation and charge recombination time constants. Details are provided in the SI (S4). Briefly, we fit the PL decays in QD-Al_2O_3@TiO_2 films and QD-TiO_2 films to extract the CS time constants. The CS time constants are calculated to be 457 ± 4 ps and 288 ± 1 ps in QD original-TiO_2 and QD washed-TiO_2 films, respectively (Table S5). The corresponding CS efficiencies are 89.9 ± 0.3% and 98.3 ± 0.01%. These CS time constants are included as constrained parameters in multiple exponential fits to the XB recovery kinetics. The fit reveals additional slow decay components that can be attributed to charge recombination (Table S6). From the fitting parameters, the average charge recombination time constants can be calculated to be 346 ± 18 ns and 1180 ± 60 ns in QD original-TiO_2 and QD washed-TiO_2 films, respectively.

In addition to affecting the electron transfer process, different ligand quantity per QD may also influence carrier dynamics within the QD. To quantify this factor, we plotted the PL decay rates (Table S7) as a function of ligand amount in Figure S8. As indicated by the red line in the figure, average PL decay rates vary with total ligand amount only slightly on Al_2O_3@TiO_2 films, whereas the decay rates of QDs on TiO_2 films (blue stars) are far above the red line, indicating that the differences of PL decay rates between QD-TiO_2 and QD-Al_2O_3@TiO_2 (Figure 4a and d) are mainly caused by ET, not by the ligand quantity per QD.

High conversion efficiency in solar cells requires fast and efficient charge separation and slow exciton recombination and charge recombination.[1] Our study shows that there exist ligands in QD-TiO_2 films prepared from both original and washed QDs, and the charge separation rate from excited QDs to TiO_2 increases with the decrease of the surface ligands. Compared to QD original/TiO_2 samples, QD washed/TiO_2

DOI: 10.1021/acs.jpcc.9b06725
J. Phys. Chem. C 2019, 123, 21415−21421

samples show that the CS rate increases by nearly a factor of 2, and CS efficiency increases by 8.4%. One possible reason is that ligands on the QD surfaces may serve as an insulating layer to reduce the strength of electronic coupling with TiO_2.[34] It is interesting to note that the electron transfer at the bulk $MAPbI_3$–TiO_2 interfaces has been reported to occur on the subpicosecond time scale,[31,35,36] much faster than the ET rate at the $CsPbI_3$ QD/TiO_2 interface studied in this work. This difference is inconsistent with the expected increase of charge separation rates in quantum confined $CsPbI_3$ QDs.[37] It can most likely be attributed to the lack of ligands at the bulk perovskite/TiO_2 interface, which enhances coupling strengths and ET rates. Interestingly, the charge recombination time is much longer in the QD washed/TiO_2 sample (1180 ± 60 ns) compared to the QD-original/TiO_2 sample (346 ± 18 ns), suggesting less recombination loss in the former. The origin of the slowing down of recombination rate in the former is not clear, but it suggests that aside from the change of coupling strength other factors that affect charge recombination rates must also exist. The comparison between washed QD and original QD indicates that purifying $CsPbI_3$ QDs with methyl acetate is necessary and beneficial for fabricating high efficiency solar cells. However, we cannot remove all the ligands from the QD surfaces because QDs suffer severe aggregation and degradation with further antisolvent washing. Other QD postsynthesis treatment procedures are needed to simultaneously enhance the charge separation rates and improve/maintain the QD stability.

CONCLUSIONS

In conclusion, we have investigated interfacial charge separation and charge recombination kinetics at the all-inorganic $CsPbI_3$ perovskite QD/TiO_2 nanoparticle interface and the influence of postsynthesis treatment by FTIR, TA, and PL decay measurements. Washing of QDs by MeOAc leads to the removal of native ligands on the QD surface according to the measured ratio of the absorbance of ligand IR to QD exciton bands on QD/TiO_2 films. The CS time constant decreases from 457 ± 4 ps in QD original/TiO_2 to 288 ± 1 ps in QD washed/TiO_2 films, corresponding to an increase of CS efficiency from 89.9 ± 0.3% to 98.3 ± 0.01%. Furthermore, the average charge recombination time constants decrease from 346 ± 18 ns to 1180 ± 60 ns in these films, which may reduce charge recombination loss. This result suggests that post-synthetic washing of QDs with MeOAc improves charge separation and recombination performances at the QD/TiO_2 interface, which may contribute to the reported improvement in solar cell efficiencies.

ASSOCIATED CONTENT

Supporting Information

The Supporting Information is available free of charge on the ACS Publications website at DOI: 10.1021/acs.jpcc.9b06725.

Sample preparations, transient absorption spectroscopy setups, and kinetics fitting (PDF)

AUTHOR INFORMATION

Corresponding Author

*E-mail: tlian@emory.edu (T. Lian). Group website: https://scholarblogs.emory.edu/lianlab/.

ORCID

Mark D. Losego: 0000-0002-9810-9834

Tianquan Lian: 0000-0002-8351-3690

Notes

The authors declare no competing financial interest.

ACKNOWLEDGMENTS

We gratefully acknowledge the financial support from the National Science Foundation (CHE-1726536). B.D.P. was supported by the Department of Defense (DoD) through the National Defense Science & Engineering Graduate Fellowship (NDSEG) Program.

REFERENCES

(1) Polman, A.; Knight, M.; Garnett, E. C.; Ehrler, B.; Sinke, W. C. Photovoltaic materials: Present efficiencies and future challenges. *Science* **2016**, *352* (6283), 4424.

(2) Green, M. A.; Emery, K.; Hishikawa, Y.; Warta, W.; Dunlop, E. D. Solar cell efficiency tables (Version 45). *Prog. Photovoltaics* **2015**, *23* (1), 1–9.

(3) Gratzel, M. The light and shade of perovskite solar cells. *Nat. Mater.* **2014**, *13* (9), 838–842.

(4) Nazeeruddin, M. K. In retrospect: Twenty-five years of low-cost solar cells. *Nature* **2016**, *538* (7626), 463–464.

(5) Boix, P. P.; Agarwala, S.; Koh, T. M.; Mathews, N.; Mhaisalkar, S. G. Perovskite Solar Cells: Beyond Methylammonium Lead Iodide. *J. Phys. Chem. Lett.* **2015**, *6* (5), 898–907.

(6) Saliba, M.; Matsui, T.; Seo, J. Y.; Domanski, K.; Correa-Baena, J. P.; Nazeeruddin, M. K.; Zakeeruddin, S. M.; Tress, W.; Abate, A.; Hagfeldt, A.; Gratzel, M. Cesium-containing triple cation perovskite solar cells: improved stability, reproducibility and high efficiency. *Energy Environ. Sci.* **2016**, *9* (6), 1989–1997.

(7) McMeekin, D. P.; Sadoughi, G.; Rehman, W.; Eperon, G. E.; Saliba, M.; Hörantner, M. T.; Haghighirad, A.; Sakai, N.; Korte, L.; Rech, B.; Johnston, M. B.; Herz, L. M.; Snaith, H. J. A mixed-cation lead mixed-halide perovskite absorber for tandem solar cells. *Science* **2016**, *351* (6269), 151–155.

(8) Saliba, M.; Matsui, T.; Domanski, K.; Seo, J.-Y.; Ummadisingu, A.; Zakeeruddin, S. M.; Correa-Baena, J.-P.; Tress, W. R.; Abate, A.; Hagfeldt, A.; Grätzel, M. Incorporation of rubidium cations into perovskite solar cells improves photovoltaic performance. *Science* **2016**, *354* (6309), 206–209.

(9) Swarnkar, A.; Marshall, A. R.; Sanehira, E. M.; Chernomordik, B. D.; Moore, D. T.; Christians, J. A.; Chakrabarti, T.; Luther, J. M. Quantum dot–induced phase stabilization of α-$CsPbI_3$ perovskite for high-efficiency photovoltaics. *Science* **2016**, *354* (6308), 92–95.

(10) Eperon, G. E.; Paterno, G. M.; Sutton, R. J.; Zampetti, A.; Haghighirad, A. A.; Cacialli, F.; Snaith, H. J. Inorganic caesium lead iodide perovskite solar cells. *J. Mater. Chem. A* **2015**, *3* (39), 19688–19695.

(11) Beal, R. E.; Slotcavage, D. J.; Leijtens, T.; Bowring, A. R.; Belisle, R. A.; Nguyen, W. H.; Burkhard, G. F.; Hoke, E. T.; McGehee, M. D. Cesium Lead Halide Perovskites with Improved Stability for Tandem Solar Cells. *J. Phys. Chem. Lett.* **2016**, *7* (5), 746–751.

(12) Sanehira, E. M.; Marshall, A. R.; Christians, J. A.; Harvey, S. P.; Ciesielski, P. N.; Wheeler, L. M.; Schulz, P.; Lin, L. Y.; Beard, M. C.; Luther, J. M. Enhanced mobility $CsPbI_3$ quantum dot arrays for record-efficiency, high-voltage photovoltaic cells. *Science Advances* **2017**, *3* (10), eaao4204.

(13) Carey, G. H.; Abdelhady, A. L.; Ning, Z.; Thon, S. M.; Bakr, O. M.; Sargent, E. H. Colloidal Quantum Dot Solar Cells. *Chem. Rev.* **2015**, *115* (23), 12732–12763.

(14) Protesescu, L.; Yakunin, S.; Bodnarchuk, M. I.; Krieg, F.; Caputo, R.; Hendon, C. H.; Yang, R. X.; Walsh, A.; Kovalenko, M. V. Nanocrystals of Cesium Lead Halide Perovskites ($CsPbX_3$, X = Cl, Br, and I): Novel Optoelectronic Materials Showing Bright Emission with Wide Color Gamut. *Nano Lett.* **2015**, *15* (6), 3692–3696.

(15) Liu, F.; Zhang, Y.; Ding, C.; Toyoda, T.; Ogomi, Y.; Ripolles, T. S.; Hayase, S.; Minemoto, T.; Yoshino, K.; Dai, S.; Shen, Q.

Ultrafast Electron Injection from Photoexcited Perovskite CsPbI3 QDs into TiO2 Nanoparticles with Injection Efficiency near 99%. *J. Phys. Chem. Lett.* **2018**, *9* (2), 294−297.
(16) Scheidt, R. A.; Kerns, E.; Kamat, P. V. Interfacial Charge Transfer between Excited CsPbBr3 Nanocrystals and TiO2: Charge Injection versus Photodegradation. *J. Phys. Chem. Lett.* **2018**, *9*, 5962−5969.
(17) Akkerman, Q. A.; D'Innocenzo, V.; Accornero, S.; Scarpellini, A.; Petrozza, A.; Prato, M.; Manna, L. Tuning the Optical Properties of Cesium Lead Halide Perovskite Nanocrystals by Anion Exchange Reactions. *J. Am. Chem. Soc.* **2015**, *137* (32), 10276−10281.
(18) Nedelcu, G.; Protesescu, L.; Yakunin, S.; Bodnarchuk, M. I.; Grotevent, M. J.; Kovalenko, M. V. Fast Anion-Exchange in Highly Luminescent Nanocrystals of Cesium Lead Halide Perovskites (CsPbX3, X = Cl, Br, I). *Nano Lett.* **2015**, *15* (8), 5635−5640.
(19) Nenon, D. P.; Pressler, K.; Kang, J.; Koscher, B. A.; Olshansky, J. H.; Osowiecki, W. T.; Koc, M. A.; Wang, L.-W.; Alivisatos, A. P. Design Principles for Trap-Free CsPbX3 Nanocrystals: Enumerating and Eliminating Surface Halide Vacancies with Softer Lewis Bases. *J. Am. Chem. Soc.* **2018**, *140* (50), 17760−17772.
(20) Park, Y.-S.; Guo, S.; Makarov, N. S.; Klimov, V. I. Room Temperature Single-Photon Emission from Individual Perovskite Quantum Dots. *ACS Nano* **2015**, *9* (10), 10386−10393.
(21) Makarov, N. S.; Guo, S.; Isaienko, O.; Liu, W.; Robel, I.; Klimov, V. I. Spectral and Dynamical Properties of Single Excitons, Biexcitons, and Trions in Cesium−Lead-Halide Perovskite Quantum Dots. *Nano Lett.* **2016**, *16* (4), 2349−2362.
(22) Noh, J. H.; Im, S. H.; Heo, J. H.; Mandal, T. N.; Seok, S. I. Chemical Management for Colorful, Efficient, and Stable Inorganic−Organic Hybrid Nanostructured Solar Cells. *Nano Lett.* **2013**, *13* (4), 1764−1769.
(23) Schulz, P.; Edri, E.; Kirmayer, S.; Hodes, G.; Cahen, D.; Kahn, A. Interface energetics in organo-metal halide perovskite-based photovoltaic cells. *Energy Environ. Sci.* **2014**, *7* (4), 1377−1381.
(24) Ravi, V. K.; Markad, G. B.; Nag, A. Band Edge Energies and Excitonic Transition Probabilities of Colloidal CsPbX3(X = Cl, Br, I) Perovskite Nanocrystals. *ACS Energy Letters* **2016**, *1*, 665−671.
(25) Xu, Y.; Schoonen Martin, A. A. The absolute energy positions of conduction and valence bands of selected semiconducting minerals. In *Am. Mineral.*, 2000; Vol. *85*, p 543.
(26) Yang, Y.; Rodriguez-Cordoba, W.; Xiang, X.; Lian, T. Strong electronic coupling and ultrafast electron transfer between PbS quantum dots and TiO2 nanocrystalline films. *Nano Lett.* **2012**, *12* (1), 303−9.
(27) Tvrdy, K.; Frantsuzov, P. A.; Kamat, P. V. Photoinduced electron transfer from semiconductor quantum dots to metal oxide nanoparticles. *Proc. Natl. Acad. Sci. U. S. A.* **2011**, *108* (1), 29−34.
(28) Ai, X.; Anderson, N. A.; Guo, J.; Lian, T. Electron Injection Dynamics of Ru Polypyridyl Complexes on SnO2 Nanocrystalline Thin Films. *J. Phys. Chem. B* **2005**, *109* (15), 7088−7094.
(29) She, C.; Anderson, N. A.; Guo, J.; Liu, F.; Goh, W.-H.; Chen, D.-T.; Mohler, D. L.; Tian, Z.-Q.; Hupp, J. T.; Lian, T. pH-Dependent Electron Transfer from Re-bipyridyl Complexes to Metal Oxide Nanocrystalline Thin Films. *J. Phys. Chem. B* **2005**, *109* (41), 19345−19355.
(30) Ai, X.; Guo, J.; Anderson, N. A.; Lian, T. Ultrafast Electron Transfer from Ru Polypyridyl Complexes to Nb2O5 Nanoporous Thin Films. *J. Phys. Chem. B* **2004**, *108* (34), 12795−12803.
(31) Marchioro, A.; Teuscher, J.; Friedrich, D.; Kunst, M.; van de Krol, R.; Moehl, T.; Gratzel, M.; Moser, J.-E. Unravelling the mechanism of photoinduced charge transfer processes in lead iodide perovskite solar cells. *Nat. Photonics* **2014**, *8* (3), 250−255.
(32) Lee, M. M.; Teuscher, J.; Miyasaka, T.; Murakami, T. N.; Snaith, H. J. Efficient Hybrid Solar Cells Based on Meso-Superstructured Organometal Halide Perovskites. *Science* **2012**, *338* (6107), 643−647.
(33) Wu, K.; Liang, G.; Shang, Q.; Ren, Y.; Kong, D.; Lian, T. Ultrafast Interfacial Electron and Hole Transfer from CsPbBr3 Perovskite Quantum Dots. *J. Am. Chem. Soc.* **2015**, *137* (40), 12792−12795.
(34) Pernik, D. R.; Tvrdy, K.; Radich, J. G.; Kamat, P. V. Tracking the Adsorption and Electron Injection Rates of CdSe Quantum Dots on TiO2: Linked versus Direct Attachment. *J. Phys. Chem. C* **2011**, *115* (27), 13511−13519.
(35) Ponseca, C. S.; Savenije, T. J.; Abdellah, M.; Zheng, K.; Yartsev, A.; Pascher, T.; Harlang, T.; Chabera, P.; Pullerits, T.; Stepanov, A.; Wolf, J.-P.; Sundström, V. Organometal Halide Perovskite Solar Cell Materials Rationalized: Ultrafast Charge Generation, High and Microsecond-Long Balanced Mobilities, and Slow Recombination. *J. Am. Chem. Soc.* **2014**, *136* (14), 5189−5192.
(36) Piatkowski, P.; Cohen, B.; Javier Ramos, F.; Di Nunzio, M.; Nazeeruddin, M. K.; Gratzel, M.; Ahmad, S.; Douhal, A. Direct monitoring of ultrafast electron and hole dynamics in perovskite solar cells. *Phys. Chem. Chem. Phys.* **2015**, *17* (22), 14674−14684.
(37) Shang, Q.; Kaledin, A.; Li, Q.; Lian, T. Size Dependent Charge Separation and Recombination in $CsPbI_3$ Perovskite Quantum Dots. *J. Chem. Phys.* **2019**, accepted.

DOI: 10.1021/acs.jpcc.9b06725
J. Phys. Chem. C 2019, 123, 21415−21421